Trans Indian Inst Met (2024) 77(6):1537–1544
https://doi.org/10.1007/s12666-023-03119-5

ORIGINAL ARTICLE

Microstructure and Mechanical Properties of the AlCrFeCoNi$_p$/AZ91D Composites After Heat Treatment

Yongsheng Chen[1] · Xiaomei Sun[2] · Xiaochen Zhang[1]

Received: 28 June 2023 / Accepted: 18 September 2023 / Published online: 11 February 2024

Abstract To enhance the comprehensive performance of Mg matrix composites, as-cast AlCrFeCoNi$_p$/AZ91D composites with different reinforcement contents were heat treated. Optical microscopy, scanning electron microscopy, and transmission electron microscopy were employed to characterize the microstructure evolution. The experimental results reveal that with the increasing content of AlCoNiCrFe particles, the average grain size of matrix and quantity of the β-$Mg_{17}Al_{12}$ phases decreased, and the morphology of β-$Mg_{17}Al_{12}$ phase changed. There was no intermetallic compound formed at the AlCrFeCoNi/α-Mg interface, and the AlCrFeCoNi particles' partial dissolution occured. After solution treatment at 673 K for 24 h and aging at 443 K for 16 h, the nominal component 10 vol.% composite obtained the best strength performance. The results demonstrated that variations in the quantity and shape of the β-$Mg_{17}Al_{12}$ phases, grain refinement strengthening, and CTE mismatch strengthening were mainly responsible for changes in the strength properties of the composites.

Keywords AlCoNiCrFe$_p$/AZ91D composites · Microstructure · Mechanical properties · Strengthening mechanism

✉ Xiaomei Sun
sunxiaomei_2011@163.com

Yongsheng Chen
chenyongsheng111@126.com

[1] College of Materials and Chemical Engineering, Heilongjiang Institute of Technology, Harbin 150050, China

[2] Harbin Welding Institute Limited Company, Harbin 150028, China

1 Introduction

In recent years, a series of studies on magnesium matrix composites (MMCs) with excellent performance have been reported. Particularly, metal particle-reinforced MMCs are good candidates for lightweight materials due to their high specific strength, high tensile and fatigue strength, and excellent machinability [1, 2]. Compared with traditional ceramic-reinforced magnesium matrix composites, metallic particle as the reinforcement has the characteristics of good dispersion in the melt, good interface wettability between magnesium matrix and reinforcement, and less porosity defects [3–5]. At present, high-entropy alloy (HEA) is a new type of particle reinforcement for MMCs, which has a high strength and plasticity. The advantage of high-entropy alloy particles in MMCs is the improvement in the interface bonding strength between Mg matrix and reinforcement particles, and high-entropy alloy particles hardly react with Mg to form brittle intermetallic compounds, which also is conducive to the enhancement of the strength of Mg matrix and not a significant loss in ductility [6–8].

Heat treatment is an effective process that changes the microstructure of magnesium matrix composites by heating, heat preservation, and cooling. As a conventional method to improve casting performance, heat treatment processing is characterized by simple process, low cost, and significant performance improvement [9–13]. Yang et al. [14] prepared TiB_2/AZ91 composites and improved their hardness and tensile strength after heat treatment process. They reported that the TiB_2 particles accelerate the precipitation behavior and generate more $Mg_{17}Al_{12}$ phase with a smaller size and clarify the improvement in mechanical properties which is mainly attributed to grain refinement strengthening mechanism and coefficient of thermal expansion mismatch strengthening mechanism. Zhang et al. [13] prepared SiC

nanoparticle-reinforced AZ91D matrix composites by using squeeze casting technology and heat treatment and reported that the aged composites had balanced tensile strength of 275 MPa and elongation of 5.1%, and 2 wt.% SiC nanoparticles content significantly improved strength and plasticity after heat treatment. They also found that the uniformly dispersed SiC nanoparticles and precipitation phase together contributed to the improvement in strength and plasticity. In the present paper, we continued to study the microstructure and mechanical properties of AlCrFeCoNi$_p$/AZ91D composites after heat treatment, and this investigation is important for developing the high-performance AlCrFeCoNi$_p$/AZ91D composites.

2 Experimental Methods

The commercially available AZ91D ingot (about Al: 8.97, Zn: 0.68, Mn: 0.22, Mg: 90.13 wt.% for the main alloying elements) was used as a matrix material, the commercialized AlCrFeCoNi particles (about Al: 8.81, Cr: 20.71, Co: 23.76, Ni: 23.62, Fe: 23.1. wt.%, supplied by Jiangsu Vilory Advanced Materials Technology Co., Ltd., China) were used as the reinforcements, and the particle size of the spherical AlCrFeCoNi particles was below 25 μm. We followed the methods given in our previous work [15] to prepare the as-cast n-AlCrFeCoNi$_p$/AZ91D composites with nominal contents of n = 0, 3, 5, and 10 vol.% volume fractions. The particle density of AlCrFeCoNi (7.6 g/cm^3) is higher than the AZ91D matrix density (1.8 g/cm^3). The AlCrFeCoNi particles have a certain segregation distribution in the AZ91D matrix. As shown in Fig. 1, four positions of the as-cast composite are selected for chemical composition analysis. We used the methods given in our previous work to calculate AlCrFeCoNi actual content. The AlCrFeCoNi particle actual content of as-cast composites is shown in Table 1, implying that the actual content of particles in AZ91D matrix is small numbers, which will hardly reduce the weight of magnesium alloy. We chose the central part of as-cast composites ingot for subsequent heat treatment experiments. The as-cast AlCrFeCoNi$_p$/AZ91D composites were solution-treated at 673 K for 24 h and quenched in water cooling at room temperature and then subjected to aged treatment at 443 K for 16 h.

The microstructure of the heat-treated AlCrFeCoNi$_p$/AZ91D composites was examined by an optical microscope (OM, Carl Zeiss A1) and a scanning electron microscope (SEM, MX2600FE) with an energy-dispersive spectrometer (EDS). The interface structure of the heat-treated composite was investigated by TEM (JEM-2010F) and high-resolution transmission electron microscopy (HRTEM Talos 240). Thin-foil samples for TEM were mechanically polished to 60 μm and then punched to 3-mm-diameter disks by conventional ion beam. The X-ray diffraction (XRD, DX-2700B) with Cu Kα radiation ($\lambda = 1.5406$ Å) was used to perform phase analysis of the composites. The uniaxial tensile and compression experiments of heat-treated AlCrFeCoNi$_p$/AZ91D composites were conducted by universal testing machine (product model INSTRON-5569) at a velocity of 0.5 mm/

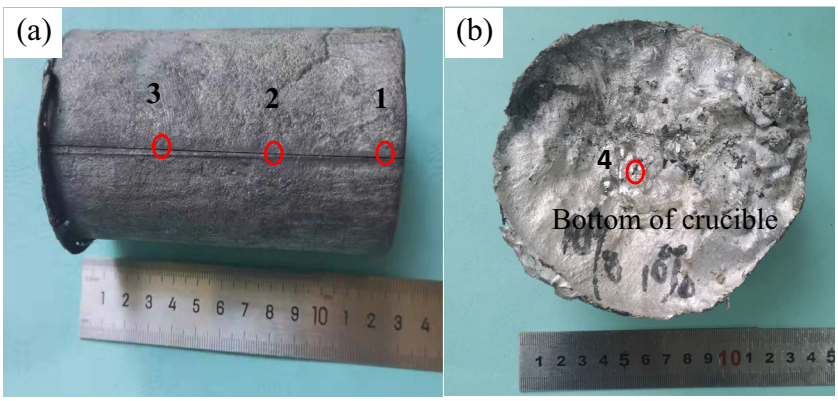

Fig. 1 Sampling positions for chemical analysis

Table 1 Chemical components of as-cast composites

Position		AZ91D + 3 vol% AlCrFeCoNi (vol.%)	AZ91D + 5 vol%	AZ91D + 10 vol%
Actual content	1	0.08%	0.08%	0.14%
	2	0.15%	0.35%	0.69%
	3	0.18%	0.38%	0.70%
	4	9.33%	12.40%	14.52%

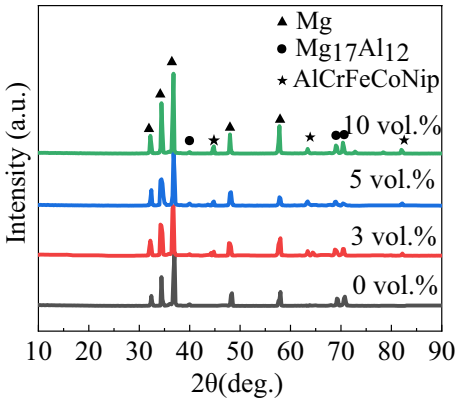

Fig. 2 XRD pattern of heat-treated AlCrFeCoNi$_p$/AZ91D composites

min at room temperature. The heat-treated samples were machined into tensile bars with a gage length of 25 and 8 mm in diameter, and at least three samples were tested for each material.

3 Results and Discussion

Figure 2 shows the XRD pattern of the heat-treated AlCrFeCoNi$_p$/AZ91D composites. All the composites samples are mainly composed of α-Mg and β-$Mg_{17}Al_{12}$ phases. With the increasing content of AlCrFeCoNi particle, the low content of AlCrFeCoNi particle phases was detectable in the XRD analysis, indicating that heat treatment will not change the phase composition.

Figure 3 shows the optical micrographs of heat-treated AlCrFeCoNi$_p$/AZ91D composites. It can be seen from Fig. 3a that the primary–secondary phases exhibit bulk

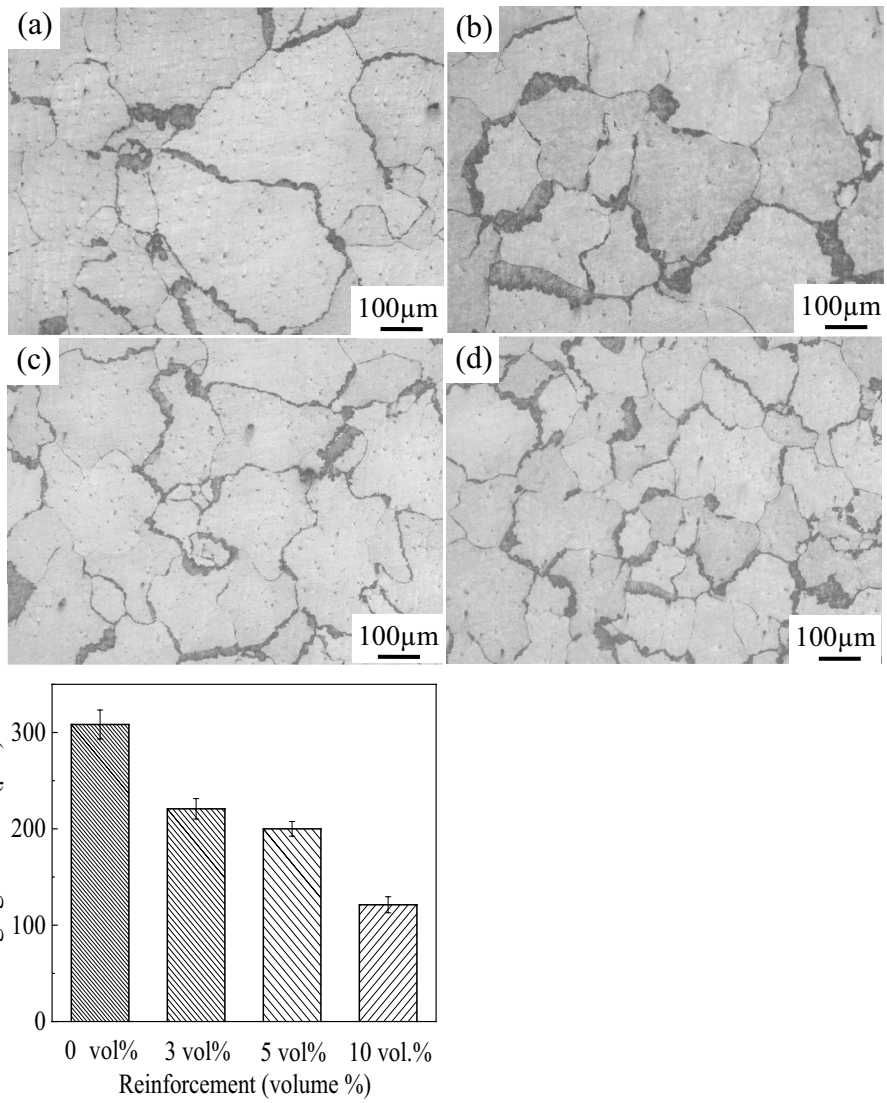

Fig. 3 Effects of particle contents on optical microstructures and average grain size images of heat-treated AlCrFeCoNi$_p$/AZ91D composites: **a** 0 vol.%, **b** 3 vol.%, **c** 5 vol.%, **d** 10 vol.%, **e** the value of average grain size

dendritic morphology and distributed along the grain boundary; with the increase content of AlCrFeCoNi particles, the bulk dendritic morphology gradually transformed into small strip shape, as shown in Fig. 3b–d. Simultaneously, it was seen that the average grain size of heat-treated composites measured using the mean linear intercept method significantly reduced from 308.3 to 121.2 μm with the addition of the AlCrFeCoNi particles from 0 to 10 vol.%, as shown in Fig. 3e. These results indicate that the AlCrFeCoNi particles have a significant refinement effect on AZ91D matrix, which is consistent with the results reported in the previous studies.

Figure 4 shows the SEM micrographs taken from the heat-treated AlCrFeCoNi$_p$/AZ91D composites. It could be seen clearly that there was no gas cavity defect in the heat-treated samples. The A and B points in Fig. 4a–d correspond to α-Mg matrix and β-$Mg_{17}Al_{12}$ phases with different morphologies, and the C points with the chemical compositions presented in the inset can be identified AlCrFeCoNi particles. It can be seen that the AlCrFeCoNi particles in the microstructures of samples often located in the grain boundaries or in the interior of the α-Mg matrix and β-$Mg_{17}Al_{12}$ phases (Fig. 4c). Simultaneously, it was seen that the bulk β-$Mg_{17}Al_{12}$ phases became a small strip shape due to the increased content of AlCrFeCoNi particles, which can also be confirmed by the OM results. Thus, this indicates that the AlCrFeCoNi particles could effectively refine the matrix.

Figure 5 shows the high-angle annular dark-field (HAADF) and corresponding EDS maps of heat-treated AlCrFeCoNi$_p$/AZ91D composites. Figure 5a shows the AlCrFeCoNi particle had partial dissolution in the melt, and the particle morphology was not circular, and the inset shows the AlCrFeCoNi particle maintained a body-centered cubic (bcc) crystal structure. It suggests that the AlCrFeCoNi particle has the high thermal stability after heat treatment process. As shown in Fig. 5b–g, it can be concluded that the elements Al, Cr, and Co diffusion exists and no intermetallic compounds were formed at the interface of AlCrFeCoNi/α-Mg, and the above results are consistent with the results of Meng et al. [16]. Figure 5h shows the high-resolution TEM (HRTEM) image of the well-bonded AlCrFeCoNi/α-Mg interface of heat-treated composites, and the interface was clean and tact. In this study, the above phenomenon may be because: (1) AlCrFeCoNi particles have hysteresis diffusion effects and the AlCrFeCoNi particles provide more low energy barriers as well as high phase and grain boundaries with high transfer coefficients, enabling effective migration of Al, Cr, and Co elements and (2) the mixing enthalpy between AlCrFeCoNi particles and magnesium matrix is relatively high, so it is difficult to form intermetallic compounds. Zhu et al. [17] studied the interface of high-entropy alloy particle-reinforced aluminum matrix composites and found that high-entropy alloy particles did not react with the aluminum matrix, and the two had a good interface bonding state. Liu et al. [8] prepared AlCrFeCoNi particle-reinforced copper matrix composites using spark plasma sintering and found that there was no chemical reaction between the AlCrFeCoNi particles and the copper matrix. Figure 5 results indicate that the interface structural characteristics of AlCrFeCoNi particle-reinforced magnesium matrix composites are different from other composite materials.

Figure 6 shows tensile true stress–strain curves of heat-treated AlCrFeCoNi$_p$/AZ91D composites. The values of strength (compression strength, yield strength, ultimate tensile strength), elongation, and Vickers hardness of

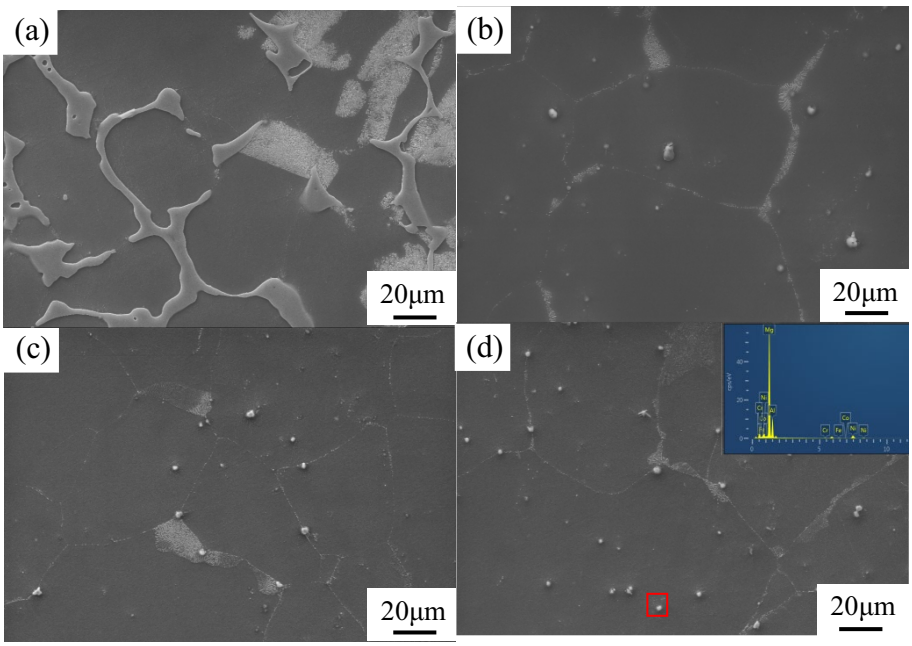

Fig. 4 Effects of particle contents on SEM images of heat-treated AlCrFeCoNi$_p$/AZ91D composites: **a** 0%, **b** 3 vol.%, **c** 5 vol.%, **d** 10 vol.%

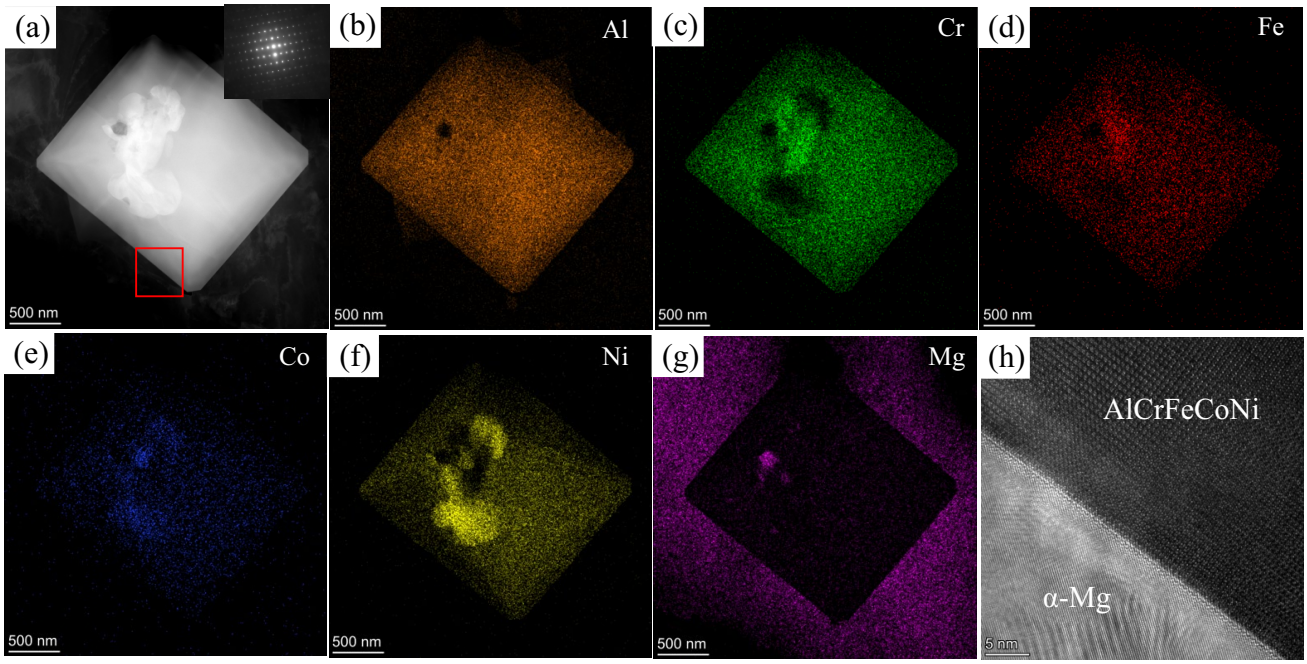

Fig. 5 HAADF image and corresponding EDS elemental maps of heat-treated AlCrFeCoNi$_p$/AZ91D samples by TEM: **a** AlCrFeCoNi particle, **b** Al, **c** Cr, **d** Fe, **e** Co, **f** Ni, **g** Mg, **h** high-magnification of AlCrFeCoNi/a-Mg interface structures in **a**

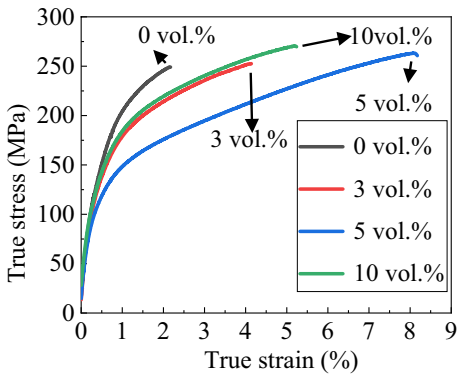

Fig. 6 The tensile curves of heat-treated AlCrFeCoNi$_p$/AZ91D composites with different particle contents

heat-treated AlCrFeCoNi$_p$/AZ91D composites are also presented in Table 2. Compared with 0 vol.% heat-treated sample, the strength and hardness were improved with the increase of the AlCrFeCoNi particles. When the volume fraction of AlCrFeCoNi particle was increased to 10 vol.%, the strength and hardness reached a maximal value. The maximum compression strength (UCS), yield strength (YS), ultimate tensile strength (UTS), and hardness values were 392.3, 117.7, 270.3 MPa, and 117.9 HV, respectively, but its elongation was only 5.2%. Conversely, the 5 vol.% heat-treated composite had the highest elongation of 8.2%, but its strength and hardness were lower than 10 vol.% samples. This indicates that the heat-treated AlCrFeCoNi$_p$/AZ91D composites in this work are difficult to achieve a simultaneous higher strength, hardness, and better ductility. The introduction of high-hardness AlCrFeCoNi particle and AlCrFeCoNi particles having a pinning effect on the grain boundary is mainly responsible for strength and hardness enhancement. In addition, AlCrFeCoNi particles impede dislocation movement, refine the grain size of the matrix, and produce fine grain strengthening effect, which are also the reasons for the increase in strength and hardness of the heat-treated composite. When the volume fraction of AlCrFeCoNi particle is 10 vol.%, a decrease in plasticity has occurred, which is because the stress concentration exists at the interface between the AlCrFeCoNi

Table 2 Effects of particle contents on mechanical properties of heat-treated AlCrFeCoNi$_p$/AZ91D composites

Composites	UCS (MPa)	0.2%YS (MPa)	UTS (MPa)	Elongation (%)	HV
0 vol.%	358.3 ± 4.2	91.2 ± 7.1	249.0 ± 6.6	2.2 ± 0.4	102.2 ± 4.2
3 vol.%	378.7 ± 2.3	109.3 ± 2.9	252.5 ± 3.1	4.1 ± 0.9	108.6 ± 2.8
5 vol.%	383.1 ± 5.3	114.0 ± 3.7	263.1 ± 2.6	8.2 ± 1.0	115.2 ± 2.4
10 vol.%	392.3 ± 5.8	117.7 ± 3.2	270.3 ± 4.2	5.2 ± 0.8	117.9 ± 4.8

particles and α-Mg matrix; the higher the particle content, the more the stress concentration, resulting in the formation of microcracks, and finally reduces the elongation of the heat-treated AlCrFeCoNi$_p$/AZ91D composite.

The mechanical properties of the heat-treated AlCrFeCoNi$_p$/AZ91D composites were apparently reinforced by the addition of the AlCrFeCoNi particles. Based on the previous research, four major strengthening mechanisms including grain refinement strengthening (Hall - Petch ,$\Delta\sigma_{Hall-Petch}$), load transfer strengthening ($\Delta\sigma_{load}$), Orowan strengthening (Orowan), and mismatch in the coefficient of thermal expansion (CTE) can effectively predict and analyze yield strength increment of heat-treated composites. The contribution of the different strengthening mechanisms could be quantitatively estimated using the following formulas [18–20]:

$$\Delta\sigma_{Hall-Petch} = k(d_{\text{composites}}^{-1/2} - d_{\text{AZ91D}}^{-1/2}) \tag{1}$$

$$\Delta\sigma_{load} = 1.5V_p\sigma_i \tag{2}$$

$$\Delta\sigma_{CET} = \sqrt{3}\alpha Gb\sqrt{\frac{12V_p\Delta C\Delta T}{(1-V_p)bd_p}} \tag{3}$$

$$\Delta\sigma_{\text{Orowan}} = \frac{\varphi Gb}{d_p}\left(\frac{6V_{\text{p}}}{\pi}\right) \tag{4}$$

$$\Delta\sigma = \sigma_{\text{Hall+}petch} + \sigma_{CET} + \sigma_{load} + \sigma_{Orowan} \tag{5}$$

where $\Delta\sigma$ is the yield strength increment, k is a constant (280 MPa μm$^{1/2}$ for AZ91D), d is the average grain sizes, α and φ are constant values of 1.25 and 2, respectively, G and b are the shear modulus (16.6 Gpa) and Burgers vector (32.1 nm) of Mg, respectively, ΔC refers to the difference in CTE between AlCrFeCoNi and Mg matrix, ΔT is the difference in temperatures between heat treatment and room temperature, and d_p and V_p are the diameter and volume fraction of AlCrFeCoNi particle, respectively [21].

The calculated results of above four contributions in yield strength of composites are shown in Fig. 7. In the present work, the grain refinement strengthening and CTE strengthening were the main strengthening mechanisms for YS enhancement. Generally, the finer grain size makes the more grain boundaries in the composites [18], and the more grain boundaries dramatically improve the probability of hindering dislocation movement, which favors the increase in yield strength of heat treatment composites. The CTE also plays an important role in strengthening the composites, and the difference of CTE between AlCrFeCoNi particles and Mg matrix induces thermal strain after heat treatment process, and high-density dislocations are produced

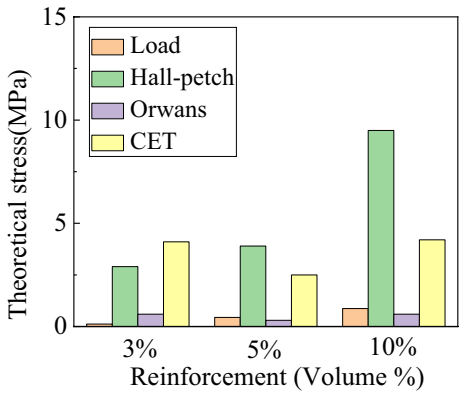

Fig. 7 The calculated contribution of individual strengthening effect to the mechanical properties

around AlCrFeCoNi particles, which eventually leads to the enhancement of yield strength. In addition, the load transfer strengthening also shows a remarkable increase in yield strength of heat treatment composites. In addition, TEM and HRTEM analysis indicates a good interface at the AlCrFeCoNi/α-Mg interface due to no intermetallic compounds formed, microcracks, and pore defects. The well-bonding AlCrFeCoNi/Mg interface favors the effective load transferring from soft Mg matrix to AlCrFeCoNi particles. At last, the enhancement effect of Orowan strengthening is relatively low due to the large size of AlCrFeCoNi particles. On comparison of theoretical values and experimental values in yield strength, we find that the theoretical values of yield strength are lower than the experimental values [22] reported that the reduced bulk β-$Mg_{17}Al_{12}$ phase content can improve the strength. We estimated the β-$Mg_{17}Al_{12}$ phase area fraction of composites by Image-Pro Plus software, and the results of β-$Mg_{17}Al_{12}$ phase area fraction of composites with nominal composition of 0 vol.%, 3 vol.%, 5 vol.%, and 10 vol.% heat treatment composites were 32.0%, 3.6%, 2.1%, and 1.6%, respectively. With the increase in the volume fraction of AlCrFeCoNi particle, the size and number of β-$Mg_{17}Al_{12}$ phase decreased. Thus, this indicates that the decreased number of β-$Mg_{17}Al_{12}$ phase also could improve the strength of heat treatment composites.

Figure 8 shows the tensile fracture morphology of the heat-treated AlCrFeCoNi$_p$/AZ91D composite at room temperature. Some tearing edges were observed on the fracture surface of the 0% heat-treated sample, indicating that the sample has a certain plasticity (shown in Fig. 8a). In Fig. 8a–d, it can be seen that with the increasing content of AlCrFeCoNi particles, there are not only fibrous tearing characteristics in the fracture, but also a large number of dimples. The dimples are formed by the growth and consolidation of voids under the sliding action, indicating that the heat-treated composite has a large plastic deformation

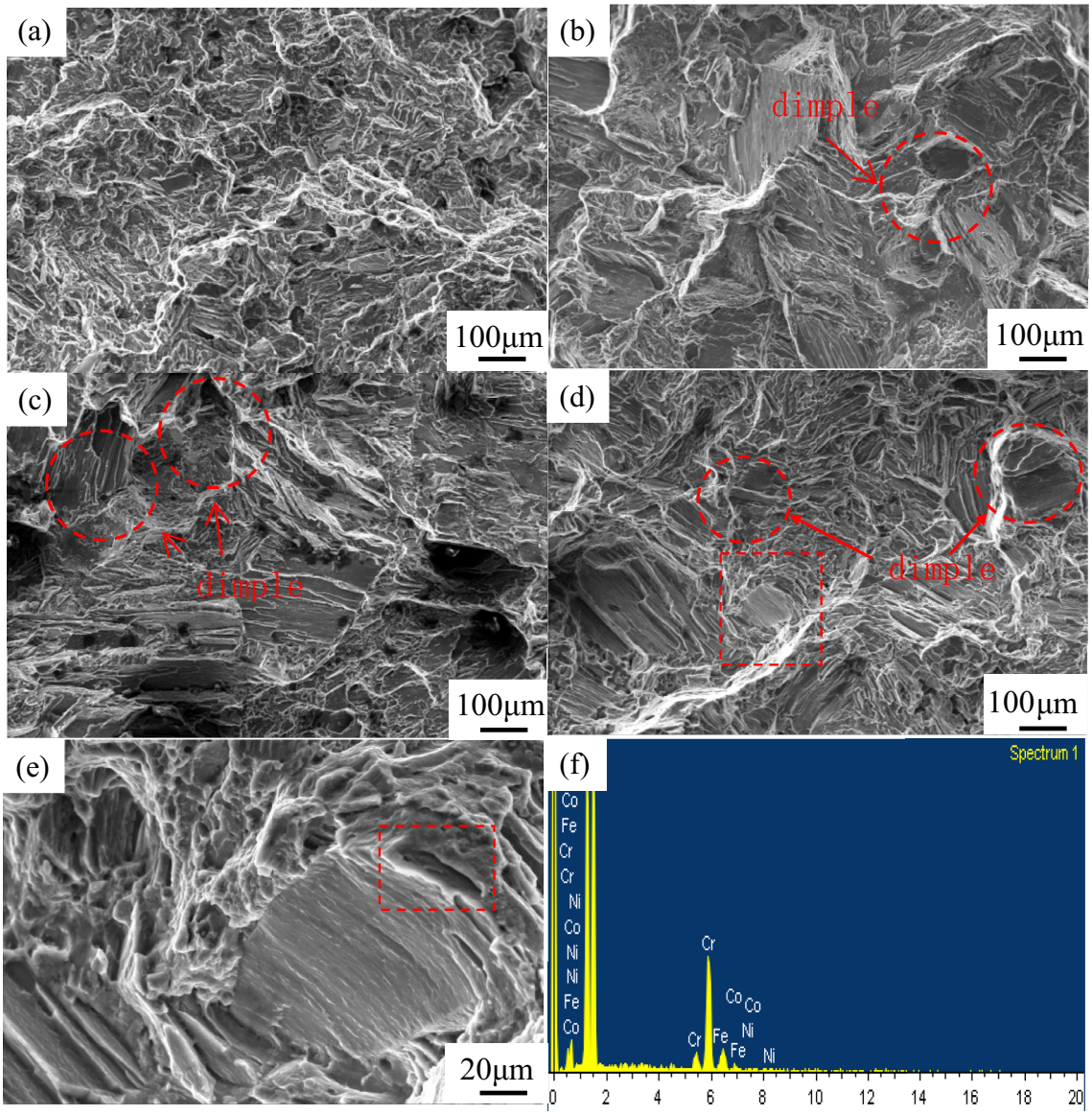

Fig. 8 Fracture surfaces of heat-treated AlCrFeCoNi$_p$/AZ91D composite with different particle contents: **a** 0 vol.%, **b** 3 vol.%, **c** 5 vol.%, **d** 10 vol.%, **e** high magnification of **d**, **f** the corresponding EDS analysis in **h**

before fracture and also indicating that the 3 vol.%, 5 vol.%, and 10 vol.% samples posses a toughness fracture structure. Figure 8e shows the enlarged area in the red box of Fig. 8d, and Fig. 8f shows the point energy spectrum in the red box of Fig. 8e. In Fig. 8e–f, we find that microcracks are initiated at the stress concentration of AlCrFeCoNi particles and matrix and often propagate along the weak interface, and then, the debonding phenomenon of AlCrFeCoNi particles and AZ91D matrix occurs, which finally causes the fracture of the composite. In other words, the finer grain size makes the more grain boundaries in the composites, which favors accommodation of plastic deformation, while the large number of AlCrFeCoNi particles induces more stress concentration, resulting in interfacial debonding; that is why the elongation of 10 vol.% composites is lower than the 5 vol.% composites.

4 Conclusion

1. With the addition of AlCrFeCoNi particles, the average grain size and numbers of β-$Mg_{17}Al_{12}$ phases of heat-treated composites were greatly reduced. AlCrFeCoNi particles have evident partial dissolution, and no intermetallic compound was formed at the AlCrFeCoNi/α-Mg interface.
2. The 10 vol.% heat-treated composites obtained outstanding strength and the hardness, and their UCS, YS, UTS,

and hardness reached 392.3 Mpa, 117.7 Mpa, 270.3 Mpa, and 124 HB, respectively. The improved strength is the results of decreased β-$Mg_{17}Al_{12}$ phases numbers, grain refinement strengthening, and CTE strengthening.

3. The influence of AlCrFeCoNi particle content on the elongation was much high, and the 5 vol.% heat-treated composite achieved an elongation of 8.2%, higher than that of 10 vol.% heat-treated composite.

Acknowledgement This work was supported by the University Nursing Program for Young Scholars with Creative Talents in Heilongjiang Province (UNPYSCT-2020033).

Declarations

Conflict of interest We declare that we have no financial and personal relationships with other people or organizations that can inappropriately influence our work, and there is no professional or other personal interest of any nature or kind in any product, service, and/or company that could be construed as influencing the position presented in, or the review of, the manuscript.

References

1. Yang H, Chen X, Huang G, Song J, She J, Tan J, Zheng K, Jin Y, Jiang B, and Pan F, *J Magnesium Alloys* (2022).
2. Pitchayyapillai G, Mohamed M J S, Dhanraj G, Prince RM, Rajeshwaran M, vMangrulkar A, *Materials Today: Proceedings* **59** (2022) 1438–1441.
3. Chen Y H, Gao X Y, Nie K B, Li YN, and Deng KK, *Materials Science and Engineering: A* **847** (2022) 143273
4. Yuan Z, Liu H, Ma Z, Ma X, Wang K, and Zhang X, *Mater Char* (2022) 111856.
5. Zhang C L, Wang X J, Wang X M, Hu X S, and Wu K, *J. Magnes. Alloy.* **4** (2016) 286–294.
6. Li J, Li Y, Wang F, Meng X, Wan L, Dong Z, and Huang Y, *Materials Science and Engineering: A* **792** (2020) 139755
7. Luo K, Xiong H, Zhang Y, Gu H, Li Z, Kong C, and Yu H, *Journal of Alloys and Compounds* **893** (2022) 162370
8. Liu Y, Chen J, Li Z, Wang X, Zhang P, and Liu J, *Vacuum* **184** (2021) 109882
9. Chen M, Fan G, Tan Z, Yuan C, Guo Q, Xiong D, Chen M, Zheng Q, Li Z, and Zhang D, *Materials Characterization* **153** (2019) 261–270.
10. Packia Antony Amalan A, Sivaram N M, Bavatharani C, and Ragupathy D, *Int J Metalcast* **16** 2022 973–986.
11. Janbozorgi M, Taheri K K, and Taheri A K, *Journal of Magnesium and Alloys* **7** (2019) 80–89.
12. Liu J A, Song D, Zhang L R, Yang X Z, Zhu X Y, Sun W B, and Chen F Y, *Journal of Materials Research and Technology* **15** (2021) 3673–3682.
13. Congyang Z, Rongyu F, and Wenzhen L, *Rare Metal Materials and Engineering* **44** (2015) 463–468.
14. Yang C C, Dong Y X, and Gao Y M, *Hot Work Technol* (2023) 1–5.
15. Chen Y S, Ji Z S, Hu M L, and Xu H Y, *Int J Mater Res* **112** (2021) 538–545.
16. Meng G, Yue T M, Lin X, Yang H, Xie H, and Ding X, *Opt Laser Technol* **70** (2015) 119–127.
17. Dezhi Z, Xia D, Longfei Q, and Qi C, *Rare Metal Mater Eng* **46** (2017) 3400–3404.
18. Ma Y, Xiong H, and Chen B, *Corrosion Science* **191** (2021) 109759
19. Abbas A, and Huang S J, *Journal of Composites Science* **5** (2021) 103.
20. Ye J, Li J, Luo H, Tan J, Chen X, Feng B, Zheng K, and Pan F, *Materials Science and Engineering: A* **833** (2022) 142526
21. Chen Y, Wang L, and Ji Z. Microstructural and Mechanical Investigations of Extruded AlCrFeCoNi/AZ91D Composites[J]. Journal of Materials Engineering and Performance, 2022: 1–10.
22. Li J M, and Deng K K, *Transactions of Materials and Heat Treatment* **33** (2012) 29–32. https://doi.org/10.13289/j.issn.1009-6264.2012.09.014